†ELECTRONIC SUPPLEMENTARY INFORMATION for:

Ball milling enables phase-pure synthesis of a temperature sensitive ternary chloride, $MgZrCl_6$

Christopher L. Rom,*[a] Austin M. Shotwell,[b] Sinclair R. Combs,[b] Autumn Peters,[c], Lauren Borgia,[c] Hannah M. Martin,[b] Michael P. Moghadasnia,[b] James R. Neilson,[c,d] and Annalise E. Maughan*[a,b]

[a] *Materials Science Center, National Laboratory of the Rockies, Golden, CO, 80401, USA. E-mail: christopher.rom@nrel.gov* [b] *Department of Chemistry, Colorado School of Mines Golden, CO, 80401, USA. Email: amaughan@mines.edu* [c] *Department of Chemistry, Colorado State University, Fort Collins, CO, 80523, USA* [d] *School of Materials Science & Engineering, Colorado State University, Fort Collins, CO, 80523, USA*

Contents

S1 Methods

S1.1 Synthesis

The precursors and products are moisture sensitive and hydrolyze rapidly on exposure to air. Thus, all work was performed in an Ar glovebox or otherwise under inert atmosphere. $MgCl_2$ (Sigma Aldrich, 99.99%, AnhydroBeads™), and $ZrCl_4$ (Thermofisher Scientific, 98%, anhydrous) precursors were used as received and were mixed 1:1 mol ratios for the various reactions. The ball milled (BM) mixture was prepared using a Fritsch Pulverisette 7 Premium ball mill with 45 mL zirconia jars and 5 mm diameter zirconia milling media (ca. 5 g sample mass, 80 g mass of milling media). Samples were milled for 50 cycles of 10 min at 500 rpm followed by a 2 min rest (10 h total milling time). We selected this procedure following our prior work on the Li-Mg-Zr-Cl system,[1] and did not assess the effect of milling conditions on the formation of $MgZrCl_6$. The hand ground (HG) mixtures were prepared by grinding the reagents with a mortar and pestle for 10 minutes. Heat treated (HT) samples of the HG and BM mixtures were prepared by first pelletizing the powders using a 6 mm die pressed at 10 MPa using a hydraulic press (ca. 400 mg per sample), then loading the pellets into quartz ampoules (10 mm ID, 12 mm OD) and flame sealing under vacuum (<30 mTorr, ca. 10 cm total sealed length). Sealed ampoules were then heated at 5 °C/min to the set point, dwelled for between 1 and 160 h, and allowed to cool naturally by turning off the furnace. Samples were then recovered in the glovebox, ground with an agate mortar and pestle, and prepared for subsequent analysis. Reagents, milled samples, and annealed samples were all colorless after grinding, indicating that reduced Zr species (e.g., $ZrCl_3$, $ZrCl_2$) are not present. Some pellets appeared grey post-reaction (Figure S1a), but we hypothesize this may stem from microstructural changes (rather than chemical changes).

S1.2 X-ray Diffraction

Laboratory X-ray diffraction was collected on a Rigaku Ultima IV and a Bruker D2 Phaser, both with Cu Kα sources. Samples were prepared on a zero-background silicon wafer and were covered with a polyimide tape to minimize exposure to oxygen and moisture. Select samples were characterized by high resolution synchrotron powder X-ray diffraction (PXRD) via the mail-in program at the Stanford Synchrotron Radiation Light Source beamline 2-1 ($\lambda = 0.729487$ Å).[2] The PXRD measurements were calibrated using a LaB_6 standard. Rietveld analysis was conducted using TOPAS Professional v6. The $MgZrCl_6$ structure was determined using the $FeZrCl_6$ structure as a starting phase (ICSD Col. Code 39666)[3] and replacing the Fe with Mg. Rietveld analysis was conducted by refining the lattice parameters, general atomic positions, atomic displacement parameters (isotropic), and crystallite size broadening (Lorentzian).

In situ synchrotron PXRD measurements were conducted at the 17-BM-B end station of the Advanced Photon Source at Argonne National Laboratory ($\lambda = 0.24101$ Å). The PerkinElmer plate detector was positioned 700 mm away from the sample. Homogenized precursors were packed into quartz capillaries in an Ar glovebox and flame-sealed under vacuum (< 30 mTorr). Capillaries were loaded into a flow-cell apparatus[4] and heated at 10 °C/min to 600 °C. Diffraction pattern images were collected every 30 s by summing 20 exposures of 0.5 s each, followed by 20 s of deadtime. Images collected from the plate detector were radially integrated using GSAS-II and calibrated using a silicon standard.

S1.3 Pair Distribution Function Analysis

Total scattering data used for pair distribution function (PDF) analysis was collected at room temperature on beamline 28-ID-1 at the National Synchrotron Light Source II (λ = 0.1665 Å). Powder samples were packed in quartz capillaries (1.1 mm outer diameter, 0.9 mm inner diameter) and flame-sealed. The data was collected using a sample-to-detector distance of ≈217.7965 mm, yielding a usable $Q_{max} = 26$ Å^{-1}, and wide-angle X-ray PerkinElmer image plate detector (2048 × 2048 array, 200 μm pixel pitch). For each sample, two images were collected and averaged where total sample exposure time was 60 s, detector exposure time was 0.5 s, and sleep time was 60 s. The detector position and alignment was calibrated using a CeO_2 (SRM674b) standard. The data was normalized into (Q) and transformed into the PDF $G(r)$ according to, $G(r) = \frac{2}{\pi}\int_{Q_{min}}^{Q_{max}} Q[S(Q)-1]\sin(Q(r))dQ$, utilizing PDFgetX3.[5] Experimental PDFs were modeled with structures derived from the crystal structure using PDFGUI.[6] Instrumental parameters, $Q_{broad} = 0.02011$ Å^{-1} and $Q_{damp} = 0.03506$ Å^{-1}, were obtained by modeling the PDF of Ni measured during the same experiment.

S1.4 Raman Spectroscopy

Raman spectra were collected on a Thermo Scientific Nicolet iS50 FTIR spectrometer with an FT-Raman module. A CaF_2 beamsplitter and InGaAs detector were employed for all reported spectra. Samples were analyzed with 0.15 W of laser intensity ($\lambda = 1064$ nm), 300 replicate scans, autogain on, and a resolution of 2 cm^{-1}. An aperture setting of 1 was necessary to eliminate detector saturation for the HT sample, while a setting of 37 was employed for all other samples. Samples were prepared by placing powdered samples on a dual concavity microscope slide and sealing the concavity with polyimide tape. Raman spectra were collected by placing the prepared microscope slides in the appropriate sample holder with the polyimide tape facing down (away from the light source). A blank microscope slide was measured under identical conditions and used for background subtraction.

S1.5 Differential Scanning Calorimetry

Differential scanning calorimetry (DSC) curves were collected on a PerkinElmer DSC 8500 using TA Instruments Tzero pans and lids. Loose powder samples of $MgZrCl_6$ (BM) were sealed in DSC pans in an argon-filled glovebox to prevent air and moisture exposure. Measurements were performed under a nitrogen purge at a flow rate of 20 mL/min. Data were collected from 50 °C to 420 °C at ramp rates of 10 °C/min (11.0 mg sample) and 40 °C/min (11.9 mg sample). DSC curves were collected for an empty pan under identical conditions for background subtraction.

S2 XRD Analysis

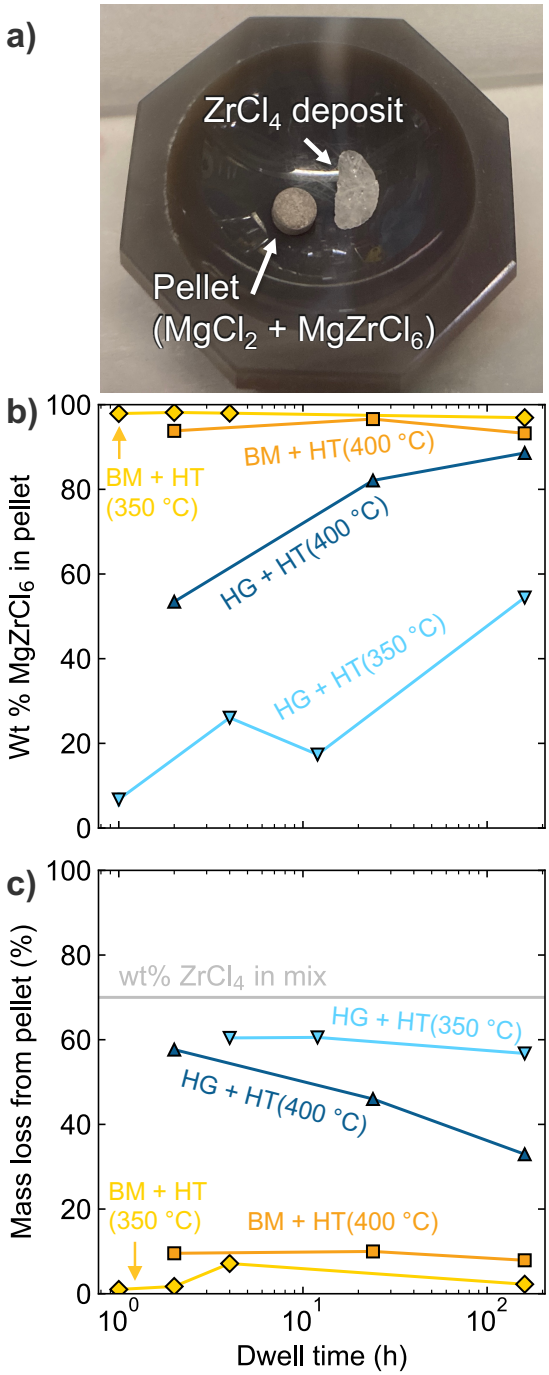

Figure S1 a) Photo of the pellet (containing $MgZrCl_6$ and $MgCl_2$) and the $ZrCl_4$ deposit recovered from a HG+HT reaction. b) Weight % $MgZrCl_6$ in the pellet determined using the Rietveld method (the remaining fraction was $MgCl_2$). c) Mass loss from the pellet as a function of synthesis condition and dwell time, compared to the weight % of $ZrCl_4$ in the precursor mix. Representative PXRD data and fits are shown in Figure S2.

Ball milling (BM) was a key synthetic step because reactions initiated from hand-ground (HG) mixtures of $MgCl_2 + ZrCl_4$ did not produce phase-pure $MgZrCl_6$ (Figure S1). Instead, HG+HT reactions yielded partial formation of $MgZrCl_6$, along with unreacted $MgCl_2$. Some of the $ZrCl_4$ transports as a vapor and deposits on the side of the ampoule (Figure S1a). At temperatures above 350 °C, BM+HT samples also lose some $ZrCl_4$, indicating that the target phase decomposes partially. This suggests that the BM+HT and the HG+HT reactions converge towards an equilibrium as temperature increases: $MgZrCl_6(s) \longleftrightarrow MgCl_2(s) + ZrCl_4(g)$. With increasing dwell time at 400 °C, the wt% of $MgZrCl_6$ in the pellet converges for the BM and HG (Figure S1b) suggesting that the reaction in the HG mixtures is kinetically limited. However, atomic-scale mixing of BM precursors allows the $MgZrCl_6$ structure to

crystallize at low temperatures (and low $ZrCl_4$ vapor pressure).

Figure S2 shows representative laboratory PXRD patterns and corresponding fits. These fits were used to calculate the phase fractions shown in Figure S1b. The BM+HT samples show consistently high phase fractions of $MgZrCl_6$ and low phase fractions of $MgCl_2$. In contrast, the HG+HT samples show a large $MgCl_2$ fraction in the 2 h synthesis, with longer dwell times leading to less $MgCl_2$ and more $MgZrCl_6$.

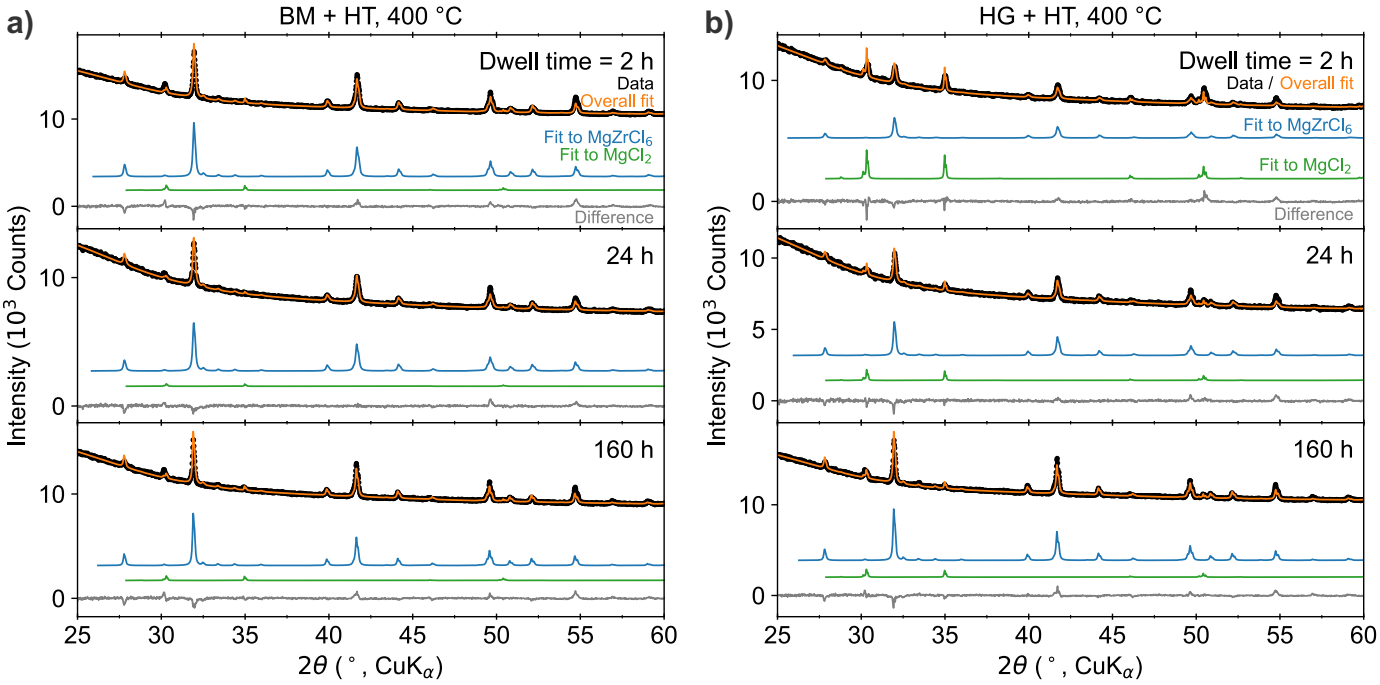

Figure S2 Representative Rietveld analysis of PXRD following the 400 ℃ heat treatments of the a) ball milled vs. the b) hand ground precursor mixes.

S3 Pair Distribution Function Analysis

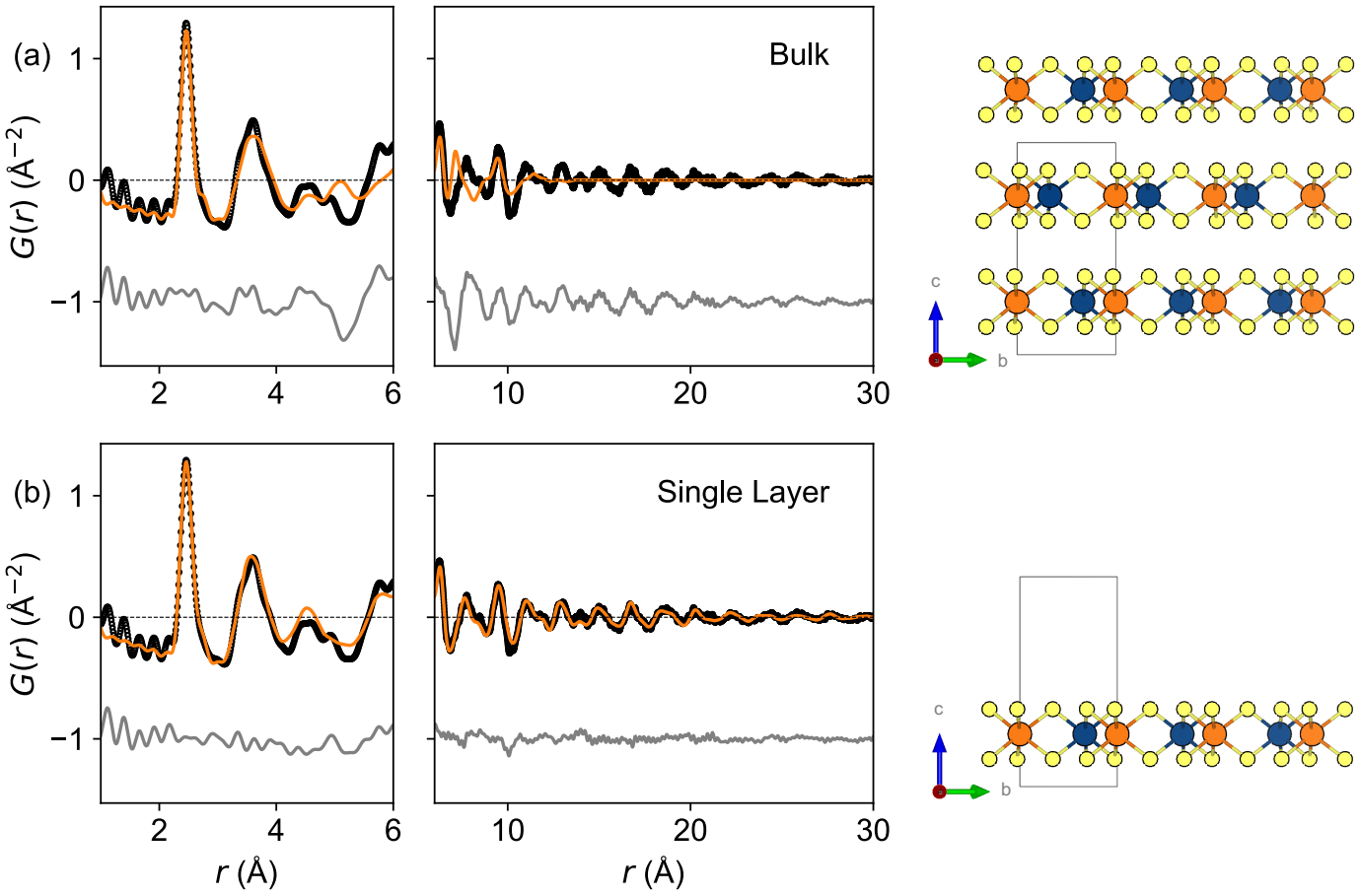

Figure S3 PDF of X-ray total scattering data from the BM sample of $MgZrCl_6$ showing two different structural models: (a) the bulk crystal structure and (b) a single layer of $MgZrCl_6$, both with spherical truncation diameter. Data in black, fit in orange, difference in gray (offset vertically by 1 Å^{-2}).

For the BM+HT sample, the bulk crystal structure produced a reasonable fit (R_w = 20.4%) for only refining a minimal number of parameters: the scale factor, correlated motion peak narrowing term (δ_1 = 2.4(1)), the lattice parameters (a = 6.35(1), c = 11.84(3)), Cl fractional coordinates (x = 0.34(1), y =0.31(1), z = 0.63(3)), and isotropic atomic displacement parameters for each element (U_{Mg} = 0.023(3) Å^2, U_{Zr} = 0.012(6) Å^2, U_{Cl} = 0.026(9) Å^2). For the BM sample, two models were tested (Figure S3). The bulk model employed for the BM+HT sample captures part of the low r pair correlations, but the model fails beyond $r \approx 4$ Å (R_w = 55.6%), as illustrated in Figure S3a. The best simple model includes only a single layer of the $MgZrCl_6$ crystal structure (R_w = 25.8%), as illustrated in Figure S3b. Following the method of Chen, et al.,[7] a composite model was constructed using a single layer of the bulk crystal structure in a unit cell with a dramatically expanded c axis and refining a minimal number of parameters (the scale factor, correlated motion peak narrowing term (δ_1 = 2.2(2)), the lattice parameters (a = 6.33(4), c = 57.42, Cl fractional coordinates (x = 0.36(1), y =0.35(2), z = 0.725), isotropic atomic displacement parameters for each element (U_{Mg} = 0.044(84) Å^2, U_{Zr} = 0.030(28) Å^2, U_{Cl} = 0.03(1) Å^2), and a spherical particle diameter (50(30) Å)). The uncertainties of the c axis and Cl z parameters are undefined, as the unit cell is artificially elongated along the c axis. As the isolated single layer alone in an artificially large unit cell has the wrong atomic number density as the synthesized compound, the sloping baseline at low r (e.g., $r < 2$ Å) and r-dependent envelope are not properly reflected with that phase alone. Correcting for these aspects is easily implemented in PDFGUI following that of Ref. 7; in summary, we include in the model a duplicated, linked second phase in the refinement with a drastically increased atomic displacement parameter to blur out the atomic correlations (U_{iso} = 0.18(13) Å^2, applied to all atoms) and a scale factor and a correlated motion parameter equal in magnitude but opposite in sign to the structural phase. This "composite" model properly corrects the sloping baseline and shape envelope and is presented in Figures 4b and S3b.

S4 Raman Spectroscopy

The raw Raman spectra of the $MgZrCl_6$ and precursor samples (Figure S4) included substantial background signal from the sample holder (Figure S5). Background subtraction was performed by subtracting the spectrum of the blank from the spectra of the samples, scaling the blank spectrum such that the large peaks from the background are no longer visible in the background-subtracted spectra. Background-subtracted Raman spectra are shown in the main body of the text (Figure 5).

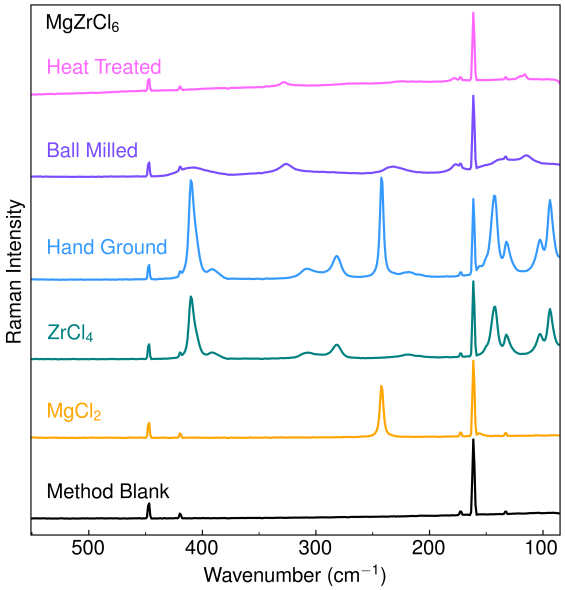

Figure S4 Raw Raman spectra of the samples shown in Figure 5 prior to background subtraction of the blank sample holder (Method Blank).

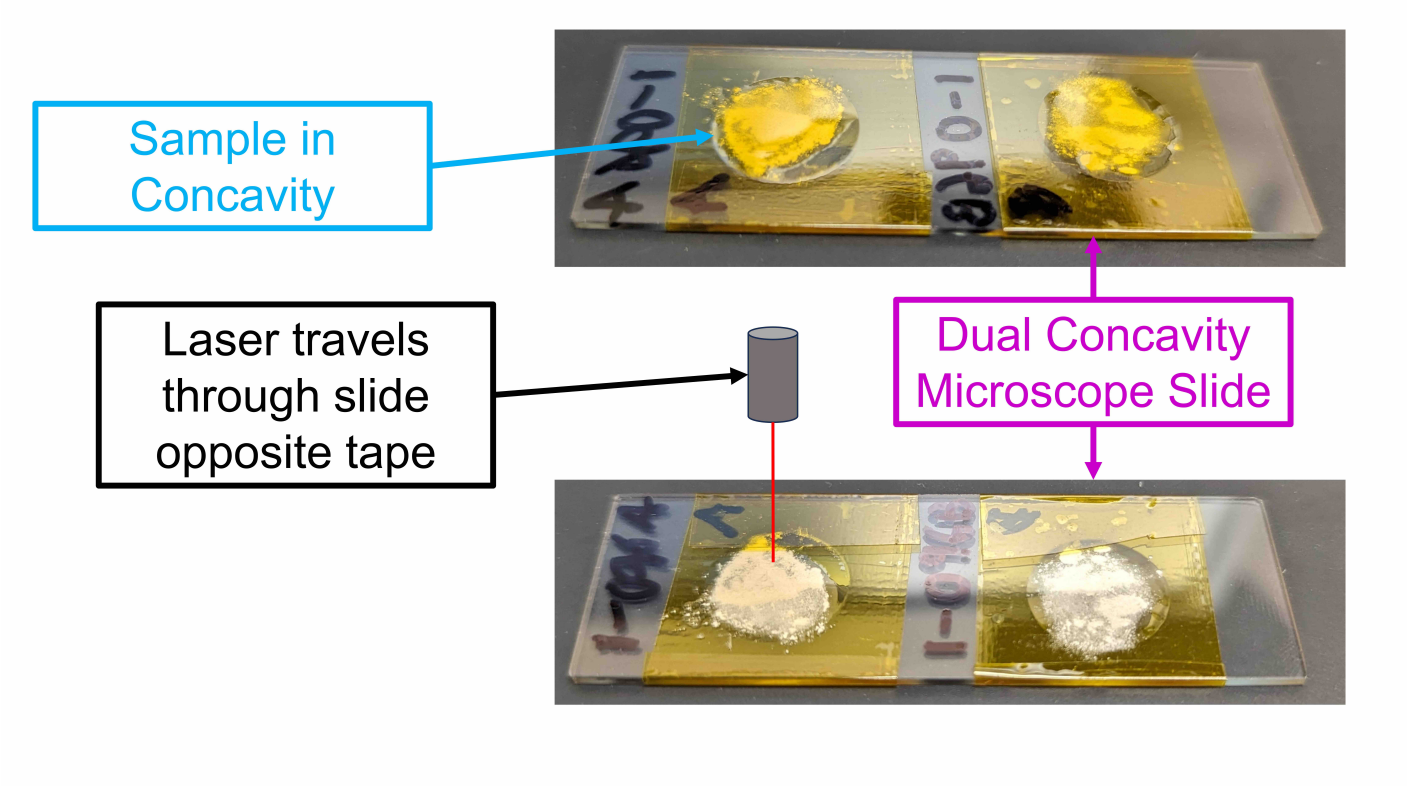

Figure S5 Diagram of the experimental setup for collecting Raman spectra.

S5 Electrochemical Impedance Spectroscopy

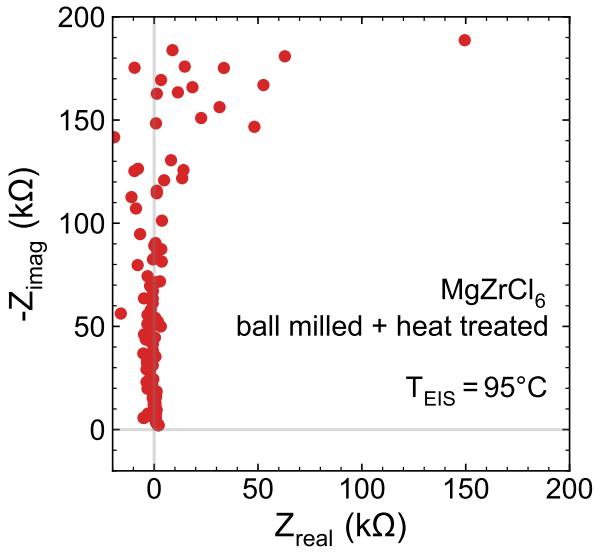

Figure S6 Nyquist plot for EIS of BM + HT $MgZrCl_6$, measured at 95 ℃.

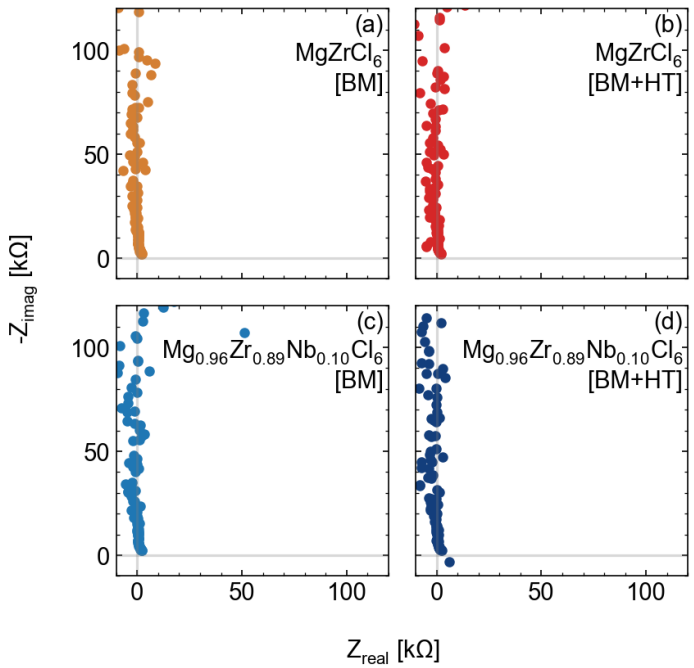

Figure S7 Nyquist plots for EIS of a) BM $MgZrCl_6$ b) BM + HT $MgZrCl_6$, c) ball milled Nb-substituted $MgZrCl_6$ and d) BM + HT sample of the Nb-substituted material. EIS was measured at 95 ℃.

Electrochemical impedance spectroscopy (EIS) measurements were performed to assess the possibility of Mg^{2+} ionic conductivity. The $MgZrCl_6$ did not exhibit measurable ionic conductivity, even at 95 °C (Figure S6). Both the ball-milled nor crystalline $MgZrCl_6$ phases exhibited behavior consistent with dielectrics (Figure S7a,b). Attempts to increase ionic conductivity via aliovalent substitution of Zr^{4+} with Nb^{5+} similarly did not yield evidence of ionic conductivity (Figure S7c,d).

S6 Bond Valence Site Energy Calculations

We turned to Bond Valence Site Energy (BVSE) calculations to provide a potential explanation for the negligibly low ionic conductivity in $MgZrCl_6$. BVSE calculations suggest that the negligibly low ionic conductivity of $MgZrCl_6$ may stem from high activation energy barriers (Figure S8). Intralayer migration barriers are calculated to be 1.77 eV. Interlayer migration has a lower barrier of 0.86 eV, but this value is still higher than the 0.6 eV cutoff used for prior theoretical work screening for Mg^{2+} ion conductors.[8] These high barriers are consistent with the prior design rules.[9,10]

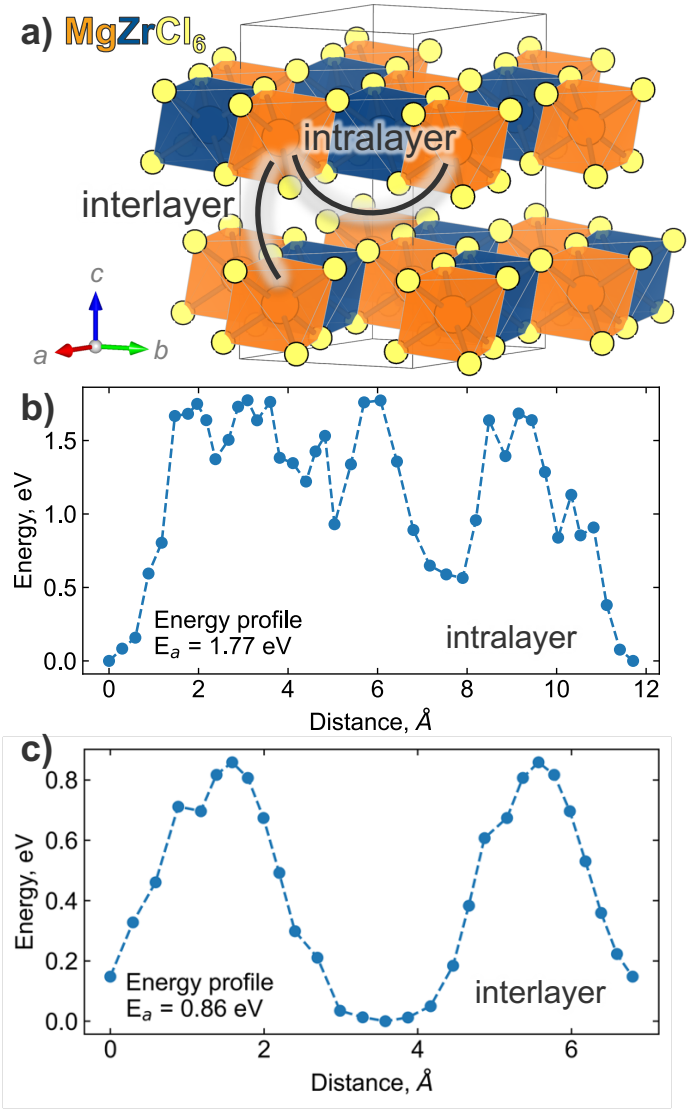

Figure S8 a) Structural model showing possible intralayer and interlayer migration pathways for Mg^{2+} in $MgZrCl_6$. BVSE calculations for b) intralayer Mg^{2+} migration show a pathway with a 1.77 eV barrier via inter-layer space and c) a lower energy pathway via interlayer migration with a 0.86 eV barrier.

S7 Differential Scanning Calorimetry

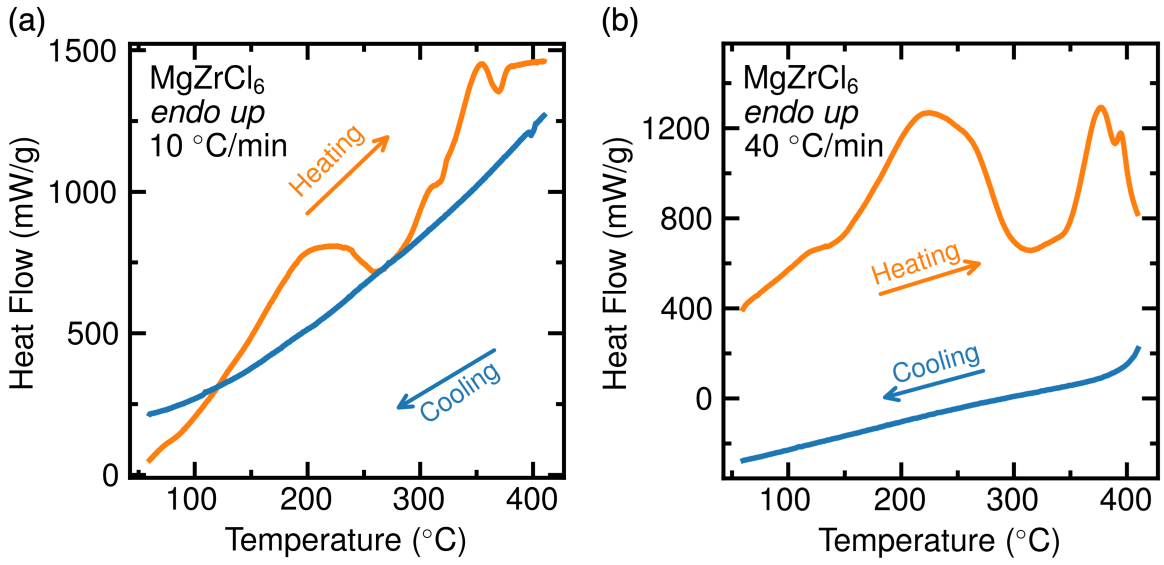

Figure S9 Differential scanning calorimetry (DSC) measurements collected on ball-milled $MgCl_2$+$ZrCl_4$ powders at rates of (a) 10 ℃/min and (b) 40 ℃/min. Data were collected first on heating and then on cooling. Separate samples were measured for the data shown in panels (a) and (b).

S8 Aged Sample

To assess if the ball-milled material undergoes aging or self-crystallization over time, we collected laboratory powder X-ray diffraction data on the ball milled $MgCl_2$+$ZrCl_4$ material after ∼3 years of storage in an Argon glove box (Figure S10).

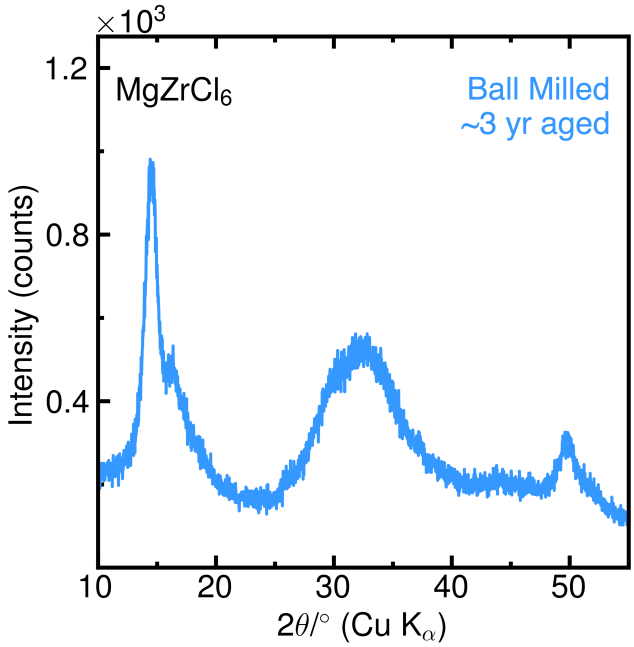

Figure S10 Laboratory powder X-ray diffraction of ball-milled $MgCl_2$+$ZrCl_4$ collected ∼3 years after the high-resolution synchrotron powder X-ray diffraction data presented in Figure 2. The sample was stored in an Ar-filled glove box.

Notes and references

[1] C. L. Rom, P. Yox, A. M. Cardoza, R. W. Smaha, M. Q. Phan, T. R. Martin and A. E. Maughan, Chem. Mater., 2024, **36**, 7283–7291.

[2] K. H. Stone, M. R. Cosby, N. A. Strange, V. Thampy, R. C. Walroth and C. Troxel Jr, J. Appl. Crystallogr., 2023, **56**, 1480–1484.

[3] S. Troyanov, B. Kharisov and S. Berdonosov, Zhurnal Neorganicheskoj Khimii, 1992, **37**, 2424–2429.

[4] P. J. Chupas, K. W. Chapman, C. Kurtz, J. C. Hanson, P. L. Lee and C. P. Grey, J. Appl. Crystallogr., 2008, **41**, 822–824.

[5] P. Juhás, T. Davis, C. L. Farrow and S. J. Billinge, Appl. Crystallogr., 2013, **46**, 560–566.

[6] C. L. Farrow, P. Juhas, J. W. Liu, D. Bryndin, E. S. Bozin, J. Bloch, T. Proffen and S. J. L. Billinge, J. Phys.: Condens. Matter, 2007, **19**, 335219.

[7] Z. Chen, M. L. Beauvais and K. W. Chapman, J. Appl. Crystallogr., 2023, **56**, 328–337.

[8] T. Chen, G. Sai Gautam and P. Canepa, Chem. Mater., 2019, **31**, 8087–8099.

[9] Z. Rong, R. Malik, P. Canepa, G. Sai Gautam, M. Liu, A. Jain, K. Persson and G. Ceder, Chem. Mater., 2015, **27**, 6016–6021.

[10] Z. W. Iton and K. A. See, Chem. Mater., 2022, **34**, 881–898.